Development of a Circuit-Type Multiple-Agile Beamforming and Interference Mitigation Network

Aslan, Yanki; Roederer, Antoine; Fonseca, Nelson J.G.; Angeletti, Piero ; Yarovoy, Alexander

DOI
10.23919/EuCAP60739.2024.10501550

Publication date
2024

Document Version
Final published version

Published in
Proceedings of the 2024 18th European Conference on Antennas and Propagation (EuCAP)

Development of a Circuit-Type Multiple-Agile Beamforming and Interference Mitigation Network

Yanki Aslan*, Antoine Roederer†, Nelson J. G. Fonseca‡, Piero Angeletti§, Alexander Yarovoy¶
*Department of Microelectronics, Delft University of Technology, Delft, The Netherlands, y.aslan@tudelft.nl
†Department of Microelectronics, Delft University of Technology, Delft, The Netherlands, roederer.antoine@gmail.com
‡Antenna and Sub-Millimetre Waves Section, European Space Agency, Noordwijk, The Netherlands, nelson.fonseca@esa.int
§RF Payloads and Technology Division, European Space Agency, Noordwijk, The Netherlands, piero.angeletti@esa.int
¶Department of Microelectronics, Delft University of Technology, Delft, The Netherlands, a.yarovoy@tudelft.nl

***Abstract*—An innovative reconfigurable beamforming network concept for multiple high-gain agile and mutually zero-forced beam generation is proposed. Four-port couplers and variable phase shifters are used to synthesize the network. A 2 beam by 7 element beam former is designed and fabricated as proof of concept. A static scenario with the two beams separated by the approximated array beamwidth is considered in the prototype. At the operating frequency of 9 GHz, based on the array factor using the measured scattering parameters, it is demonstrated that the null levels stay below -37 dB, while the beam weights remain close to uniform for the best efficiency.**

***Index Terms*—beamforming, interference suppression, multi-beam antenna, phased array, zero-forcing.**

I. Introduction

Modern communication and sensing systems increasingly require transmit/receive antennas capable of generating multiple simultaneous agile beams to provide desired coverage, angular resolution and spectral efficiency demands [1]. The high complexity and cost of multiple beam generation via fully-digital beamforming motivates the use of analog multibeam antennas and hybrid beam forming architectures employing analog multibeam subarrays [2]. The typical and future applications of these beamformers include base station antennas with multiple beams in the elevation and/or azimuth planes [3], [4], multibeam mobile phones [5], [6], radars (military, automotive, weather etc.) with anti-jamming and multi-functionality [7], [8], radio telescopes with multiple independent beams observing different regions in the sky simultaneously [9], and satellite communication antennas for both space and ground segments with tracking and smooth handover capabilities [10]–[12].

The traditional fixed beamforming networks (BFNs), such as Blass, Butler and Nolen matrices, and their hybrid forms [13], do not have the ability to scan the multiple beams independently, which limits their suitability in the above-mentioned applications. Besides, for optimal link quality, the interference between the simultaneously formed reconfigurable co-frequency beams must be cancelled via zero-forcing (ZF), or similar type of adaptive pattern nulling techniques [14].

Several examples of analog reconfigurable matrices with relatively small number of elements and concurrent beams (up to 4), and with interference cancellation functionality can be found in the literature [15], [16]. In these studies, chip-scale multibeam front-ends and hybrid architectures employing analog beamforming integrated circuits (ICs) were used with adders [17]. Therefore, they suffer from large RF signal combining losses. It remains an open research and engineering challenge to generate and maintain multiple adaptive simultaneous beams with high power efficiency, wide scan angle and limited interference.

Towards this aim, the concept of Generalized Joined Coupler (GJC) matrix was introduced with a theoretical discussion on its implementation in Blass and Nolen matrices with variable phase shifters (VPSs). The goal was to achieve individual beam steering function [18]. However, the interference-mitigation was limited to peak sidelobe level (PSLL) control by adjusting the array tapering with the fixed coupling ratios [19], which increases the beamwidth and reduces the gain.

To resolve this issue, we recently proposed: (i) a modified unit cell with 4-port tunable combining modules integrating a coupler with VPSs [20], and (ii) an innovative high-gain agile orthogonal and ZF beams synthesis strategy [21]. In this paper, complementary to our recent work, we present a novel 2 beam by 7 element BFN prototype as proof of concept, which demonstrates the key idea behind our new beamforming approach and validates its practical efficacy.

The rest of the paper is organized as follows. Section II describes the topology of the BFN, its working principle and beam synthesis procedure. Section III explains the design methodology applied in the simulations and fabricated printed circuit board (PCB). Section IV discusses the BFN performance with a comparison of synthesized, full-wave simulated and measured results. Section V concludes the paper.

II. BFN Synthesis

The principle of the proposed 2 ZF beam by 7 element BFN, best seen in the receive (Rx) mode, is schematically illustrated in Fig. 1. It is worth noting that the principle is also applicable to the transmit (Tx) mode by reciprocity [14].

For basic concept demonstration, the following simplifying assumptions are made in the synthesis procedure:

- Isotropic antenna elements are used. The focus is on the array factor. The work can be extended with inclusion of

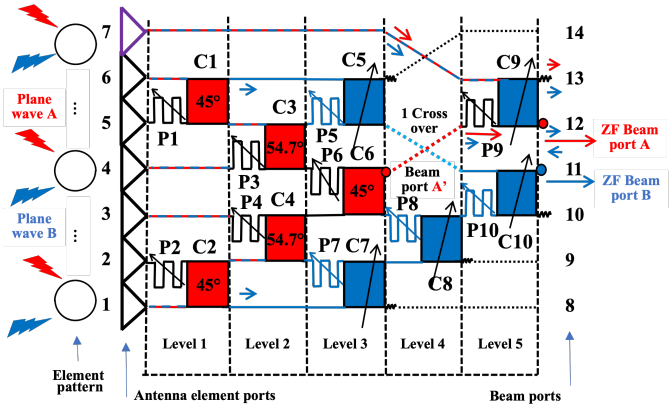

Fig. 1. Schematic of the proposed 2 ZF beam by 7 element BFN in Rx mode.

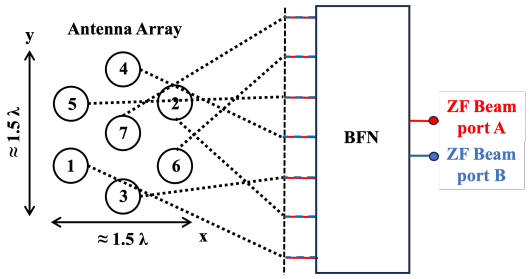

Fig. 2. The antenna array topology associated with the proposed BFN.

mutual coupling via embedded element patterns obtained via full-wave simulation or measurements of the array.

- The lines, couplers and phase shifters are assumed to be lossless. An angle (α) is assigned to each coupler representing the coupling ratio. Going through a coupler multiplies the signal amplitude with $\cos\alpha$, while going across means multiplication with $\sin\alpha$.
- Going through a straight or oblique line has 0^o phase shift.
- Going through the cross-over (across) has 0^o phase shift. Going through a coupler has 0^o phase shift for straight and -90^o phase shift for across.

In Rx, the incident A and B plane waves must be weighted accordingly. In this work, we assume a circular array topology with half-wavelength (0.5λ) spacing as visualized in Fig. 2. The red couplers (C1-2-3-4-6) are fixed (in the case of identical element patterns, as we assume), and they are set to direct Port-1 to Port-6 entering red signal to the beam port A'. No red signals then enter to C5-7-8-10. These blue tunable couplers and associated VPSs are set to direct all blue signals entering them to Port-11, called the ZF beam port B. Finally, C9 and its VPS are set for entering signal from Port-7 from plane wave B to cancel the blue signal at Port-12, called the ZF beam port A.

For high-gain ZF beams with close-to-uniform weights, it is crucial that the angular spacing between the beams is larger than the array beamwidth [20]–[22]. In this work, to demonstrate our reconfigurable BFN concept in a static scenario, we assume $1.0\lambda/D$ angular separation between the two beams,

TABLE I
THE SYNTHESIZED BFN FOR A SAMPLE CASE WITH $1.0\lambda/D$ BEAM SEPARATION IN THE uv-PLANE ($u_A = v_A = -0.03, u_B = v_B = -0.5$).

Coupler label	Coupling angle (°)	Phase shifter label	Phase shift (°)
C1	45.0	**P1**	-93.8
C2	45.0	**P2**	-75.9
C3	54.7	**P3**	-176.7
C4	54.7	**P4**	-178.1
C5	35.4	**P5**	-142.4
C6	45.0	**P6**	-81.1
C7	54.1	**P7**	-152.1
C8	49.7	**P8**	-52.4
C9	22.6	**P9**	-7.0
C10	58.6	**P10**	-8.9

where λ is the wavelength at the center frequency of operation and D is the array diameter. In the uv-plane, one ZF beam peak is randomly positioned at $u_B = v_B = -0.5$, while the other ZF beam peak is positioned at $u_A = v_A = -0.03$, with the distance being equal to 0.67 for $D = 1.5\lambda$. Next, by following the proposed synthesis approach, the coupling angles (α's) and phase shifts for the 5 tunable couplers and 10 VPSs are determined. The result is given in Table I.

III. BFN Design

The values in Table I and the assumptions made in the BFN synthesis procedure are used as inputs in the design of the synthesized BFN. Our design, which is not optimal in terms of the total length and losses of the BFN but still sufficient as a proof-of-concept, applies the following strategy:

- The design is realized at 9 GHz operating frequency in low-cost single-layer microstrip line technology. However, the concept is applicable to different frequencies and design technologies, including digital beamforming. Maintaining ZF within a frequency band remains an open challenge.
- Taconic TLY-5 [23] with the relative permittivity of 2.2 is used as the substrate. The substrate thickness is 0.508 mm. The copper thickness for the lines and the ground plane is 0.035 mm. The $50\,\Omega$ lines have the width of 1.5 mm.
- Each coupler, connector board and terminations are separately tuned and later combined.
- Same cell length and width is assumed for all cells with/without coupler at each level (level length is larger when there is a tunable coupler in the cell).
- Phase shifting lines are placed to the left of each coupler on both arms to achieve phase equalization within each level (as assumed in the synthesis) and to obtain the required phase difference between the arms as given in Table I.
- In the phase shifter lines, 4 turns are used in most cells for simple tuning, where only the height is adjusted. Mitered bends are used to minimize the reflections.
- Variable couplers are realized with two back-to-back 3 dB (i.e. $\alpha = 45^o$) couplers with a phase shift line in between (single turn, with adjusted height). The cross over is also realized with two back-to-back 3 dB couplers.

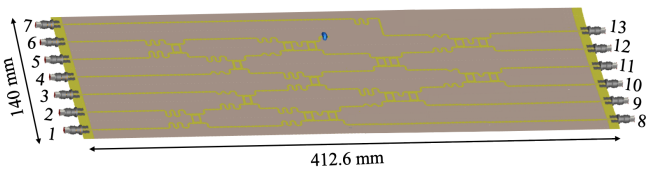

(a)

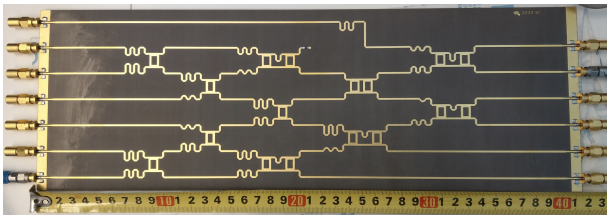

(b)

Fig. 3. Design of the synthesized BFN: (a) simulation model in CST Microwave Studio, (b) fabricated board.

- During parameter tuning, the coupler is excited from a port on the right-hand-side (which aligns with the arm where there is no additional phase shift), and amplitude and phase of transmission coefficients are observed.
- To prevent potential issues in hand soldering, the terminations (except one in Level 4, next to C5) are extended to the board edge where connectors with a matched load are placed. The remaining termination is realized by a $50\,\Omega$ SMD resistor (metric 2012, from Vishay) on an open ended line.
- The SMA PCB edge launch connector from Amphenol SV Microwave (part number 2921-61493) is used at Ports 1 to 13. The connector footprint is optimized with a smooth transition to the $50\,\Omega$ line for minimal reflection at 9 GHz.
- The line lengths are extended in the cells with the connectors. This was made for potential need for post-calibration, which was not necessary in the end.

This strategy yields the complete BFN shown in Fig. 3, with the full-wave CST simulation model given in Fig. 3a, and the fabricated and assembled PCB photographed in Fig. 3b.

IV. BFN Performance

To assess the BFN performance in terms of the radiation patterns, the scattering (S-) parameters (S1,12 to S7,12 for ZF beam A, and S1,11 to S7,11 for ZF beam B) are determined. Then, the array factor is computed and standard directivity formula is applied. The synthesized S-parameters are obtained in MATLAB by following the BFN synthesis procedure explained in Section II. The full-wave simulated S-parameters are extracted from CST simulations of the BFN model shown in Fig. 3a. For the measured S-parameters, the setup shown in Fig. 4 is used. Calibrated two ports of the Keysight P9374A vector network analyzer (VNA) are sequentially connected to the BFN Ports 1 to 7 and 11 and 12, respectively. The remaining BFN ports are terminated by $50\,\Omega$ loads.

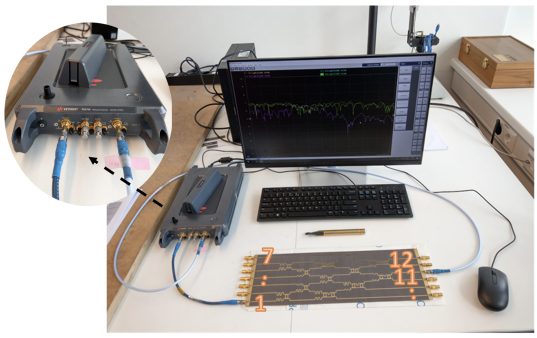

Fig. 4. The measurement setup for the BFN S-parameters characterization.

TABLE II
COMPARISON OF THE SYNTHESIZED, FULL-WAVE SIMULATED AND MEASURED BEAM WEIGHTS AT 9 GHZ.

		Synthesized		CST simulated		Measured	
		Amp.	**Ph. (°)**	**Amp.**	**Ph. (°)**	**Amp.**	**Ph. (°)**
ZF Beam A	**S1,12**	0.377	0.00	0.329	0.00	0.231	0.00
	S2,12	0.377	14.06	0.282	14.70	0.220	18.41
	S3,12	0.377	1.88	0.280	7.01	0.239	2.18
	S4,12	0.377	12.18	0.251	22.95	0.237	19.22
	S5,12	0.377	5.15	0.242	7.92	0.202	12.35
	S6,12	0.377	8.92	0.307	11.34	0.226	12.56
	S7,12	0.384	187.03	0.307	205.36	0.253	192.12
ZF Beam B	**S1,11**	0.450	0.00	0.307	0.00	0.261	0.00
	S2,11	0.450	262.07	0.319	259.32	0.255	258.36
	S3,11	0.414	31.29	0.317	33.76	0.253	30.75
	S4,11	0.414	230.78	0.354	230.08	0.266	231.79
	S5,11	0.356	92.24	0.235	78.91	0.189	88.51
	S6,11	0.356	169.83	0.272	173.28	0.206	171.14
	S7,11	0.000	132.92	0.006	115.08	0.005	102.17

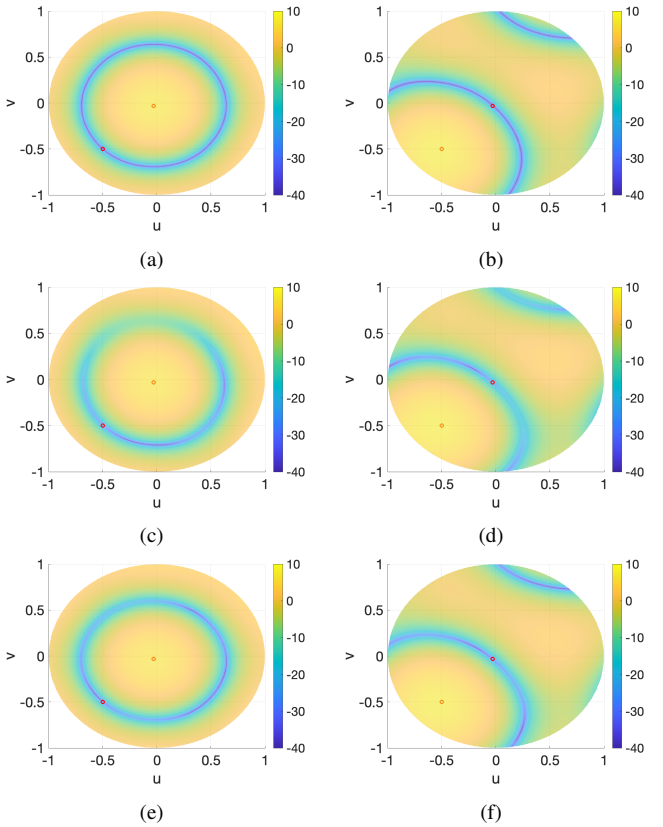

Fig. 5. Directivity (in dBi) array factor uv-plane patterns: (a) ZF beam A - synthesized, (b) ZF beam B - synthesized, (c) ZF beam A - simulated, (d) ZF beam B - simulated, (e) ZF beam A - measured, (f) ZF beam B - measured.

TABLE III

COMPARISON OF THE DIRECTIVITY (IN DBI) AT THE TWO BEAM POSITIONS BASED ON THE SYNTHESIZED, SIMULATED AND MEASURED S-PARAMETERS.

	Synthesized		**Full-wave simulated**		**Measured**	
	Directivity (dBi) $(u_A = v_A = -0.03)$	**Directivity (dBi)** $(u_B = v_B = -0.5)$	**Directivity (dBi)** $(u_A = v_A = -0.03)$	**Directivity (dBi)** $(u_B = v_B = -0.5)$	**Directivity (dBi)** $(u_A = v_A = -0.03)$	**Directivity (dBi)** $(u_B = v_B = -0.5)$
ZF Beam A	6.61	-74.98	6.36	-26.02	6.22	-35.24
ZF Beam B	-41.95	7.19	-24.10	7.21	-29.75	7.20

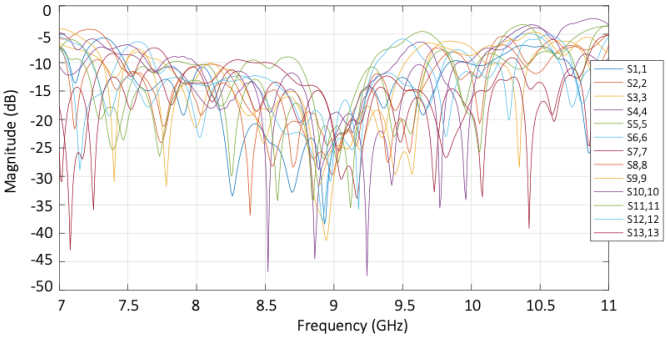

Fig. 6. The measured reflection coefficients of the BFN.

The comparison of S-parameters at the design frequency of 9 GHz in the case of synthesized, full-wave simulated and measured results is listed in Table II. It is worth noting that the phase at Port 1 of the BFN is taken as a reference in each case for easy comparison. From Table II, it is apparent that there is an excellent agreement between the synthesized, simulated and measured weights. However, the impact of slight amplitude and phase differences on the ZF beam patterns (especially on the depth of nulls) is yet to be evaluated. Therefore, the directivity patterns are plotted in Fig. 5 for each case. It is seen that despite the non-idealities as compared to the synthesized results, the null levels are still at -32.4 dB and -31.3 dB for the two ZF beams in the CST simulations. Moreover, there is very good pattern agreement in the measured results, also with improved null depths, to -41.5 dB and -37.0 dB, respectively. The maximal directivities are similar in the case of synthesized, simulated and measured beam weights.

Lastly, the nulling performance within a 800 MHz band is studied. The measured reflection coefficients of the BFN are plotted in Fig. 6. In addition to the previous S-parameter results at 9 GHz, the S-parameters at 8.6 GHz, 8.8 GHz, 9.2 GHz and 9.4 GHz are used here (not tabulated in the paper for brevity). The corresponding directivity patterns for the two ZF beams are shown in Fig. 7. The key results in terms of the null depths are summarized in Table IV. It is seen that for ZF beam B, the nulls are maintained at a low

TABLE IV

DIRECTIVITY (IN DBI) AT THE TWO BEAM POSITIONS BASED ON MEASURED S-PARAMETERS AT DIFFERENT FREQUENCIES.

	8.6 GHz	**8.8 GHz**	**9.0 GHz**	**9.2 GHz**	**9.4 GHz**
	Directivity (dBi) $(u_A = v_A = -0.03)$				
ZF beam A	5.81	6.03	6.22	6.35	6.82
ZF beam B	-26.15	-26.75	-29.75	-27.96	-19.00
	Directivity (dBi) $(u_B = v_B = -0.5)$				
ZF beam A	-5.47	-10.58	-35.24	-11.53	-7.75
ZF beam B	6.58	7.04	7.20	7.05	6.74

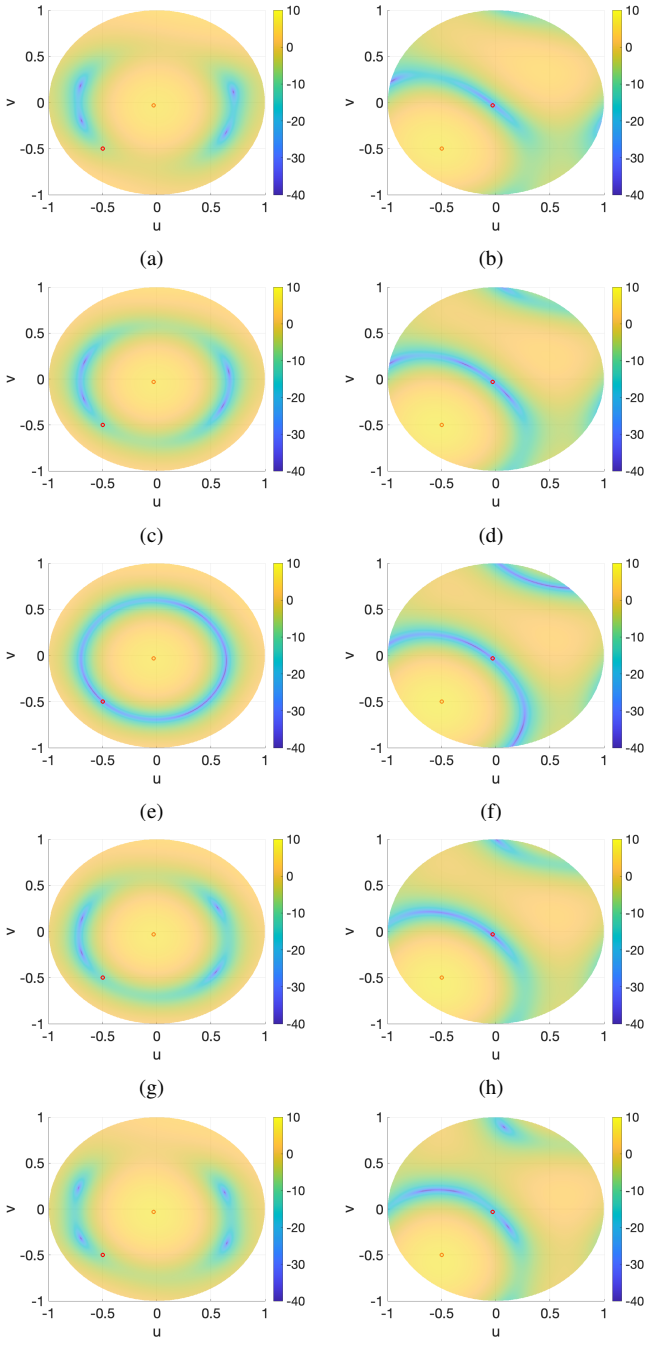

Fig. 7. Directivity (in dBi) array factor uv-plane patterns from the measured S-parameters at different frequencies: (a) ZF beam A - 8.6 GHz, (b) ZF beam B - 8.6 GHz, (c) ZF beam A - 8.8 GHz, (d) ZF beam B - 8.8 GHz, (e) ZF beam A - 9 GHz, (f) ZF beam B - 9 GHz, (g) ZF beam A - 9.2 GHz, (h) ZF beam B - 9.2 GHz, (i) ZF beam A - 9.4 GHz, (j) ZF beam B - 9.4 GHz.

level (below -30 dB for 8.6 to 9.2 GHz, and below -25 dB at 9.4 GHz). For ZF beam A, on the other hand, the null is very sensitive with respect to the frequency change (reaches to -11.3 dB at 8.6 GHz). This behavior is directly related to the stability of the amplitude-phase response of the BFN against the frequency change, which can be further optimized by modifying the synthesis and/or design strategy (out of scope of this paper).

V. Conclusion

A novel BFN synthesis methodology for orthogonal and also ZF array beams is proposed. This requires, for each beam, extra dedicated array elements, couplers and variable phase shifters to adaptively suppress co-channel inter-beam interference. These networks have no inherent insertion losses: all power in is radiated out, unlike conventional analog multiple beamforming networks with high beam signal combining losses at element chain level. Depending on beam-spacing with respect to the array resolution, and also on the number of beams, synthesized illuminations might strongly reduce the gain. Therefore, the number of beams and beam directions must be carefully chosen.

Using the new proposed concept, a 2 ZF beams (with a separation of array resolution) by 7 element beam former has been designed, simulated, manufactured and tested. The array factor directivity contour plots obtained from the measured beamformer S-parameters have shown that the null level is below -37 dB at the design frequency (9 GHz), which can be highly sensitive to bandwidth.

Future work aims for (i) reconfigurable, wideband and modular implementation of the BFNs, (ii) optimally designed/selected antenna topologies, (iii) inclusion of antenna arrays and mutual coupling, and (iv) adaptation to various types of applications (5G/6G, radar, Satcom).

Acknowledgment

This work was supported by the European Space Agency (ESA) in the frame of the Open Space Innovation Program (OSIP) project titled “A key to 5G & 6G Flexible Space Connection: Antenna Butler-like Multiple Beam Forming” under Contract 4000131563.

The authors would like to thank CIMULEC Groupe, France for the fabrication of the PCB. The authors also acknowledge, with thanks, the support of F. van der Zwan and P. J. Aubry from TU Delft in PCB assembly and measurements of S-parameters.

References

[1] W. Hong, Z. H. Jiang, C. Yu, J. Zhou, P. Chen, Z. Yu, H. Zhang, B. Yang, X. Pang, M. Jiang, Y. Cheng, M. K. T. Al-Nuaimi, Y. Zhang, J. Chen, and S. He, “Multibeam antenna technologies for 5G wireless communications,” *IEEE Transactions on Antennas and Propagation*, vol. 65, no. 12, pp. 6231–6249, 2017.

[2] Y. Aslan and A. Roederer, “Multiple beam forming schemes for user terminal antennas: Now and next,” *Reviews of Electromagnetics*, 2023, submitted for publication.

[3] Y. Aslan, J. Puskely, A. Roederer, and A. Yarovoy, “Active multiport subarrays for 5G communications,” in *IEEE-APS Topical Conference on Antennas and Propagation in Wireless Communications (APWC)*, 2019, pp. 298–303.

[4] Y. Hu and W. Hong, “A novel hybrid analog-digital multibeam antenna array for massive MIMO applications,” in *IEEE Asia-Pacific Conference on Antennas and Propagation (APCAP)*, 2018, pp. 42–45.

[5] Q.-L. Yang, Y.-L. Ban, K. Kang, C.-Y.-D. Sim, and G. Wu, “SIW multibeam array for 5G mobile devices,” *IEEE Access*, vol. 4, pp. 2788–2796, 2016.

[6] Q.-L. Yang, Y.-L. Ban, J.-W. Lian, L.-H. Zhong, and Y.-Q. Wu, “Compact SIW 3×3 butler matrix for 5G mobile devices,” in *International Applied Computational Electromagnetics Society Symposium (ACES)*, 2017, pp. 1–2.

[7] F. Liu and C. Masouros, “Hybrid beamforming with sub-arrayed MIMO radar: Enabling joint sensing and communication at mmWave band,” in *ICASSP 2019 - IEEE International Conference on Acoustics, Speech and Signal Processing (ICASSP)*, 2019, pp. 7770–7774.

[8] D.-W. Kang, K.-J. Koh, and G. M. Rebeiz, “A ku -band two-antenna four-simultaneous beams SiGe BiCMOS phased array receiver,” *IEEE Transactions on Microwave Theory and Techniques*, vol. 58, no. 4, pp. 771–780, 2010.

[9] G. W. Kant, P. D. Patel, S. J. Wijnholds, M. Ruiter, and E. van der Wal, “EMBRACE: A multi-beam 20,000-element radio astronomical phased array antenna demonstrator,” *IEEE Transactions on Antennas and Propagation*, vol. 59, no. 6, pp. 1990–2003, 2011.

[10] G. He, X. Gao, L. Sun, and R. Zhang, “A review of multibeam phased array antennas as LEO satellite constellation ground station,” *IEEE Access*, vol. 9, pp. 147 142–147 154, 2021.

[11] M. J. Gonzalez, A. Pellon, and A. Ruiz, “Smart apertures for in-flight electronically steerable antennas in LEO/MEO/GEO satellite constellations,” in *16th European Conference on Antennas and Propagation (EuCAP)*, 2022, pp. 1–4.

[12] J. Palacios, N. González-Prelcic, C. Mosquera, T. Shimizu, and C.-H. Wang, “A hybrid beamforming design for massive MIMO LEO satellite communications,” *Frontiers in Space Technologies*, vol. 2, p. 696464, 2021.

[13] Y. J. Guo, M. Ansari, and N. J. G. Fonseca, “Circuit type multiple beamforming networks for antenna arrays in 5G and 6G terrestrial and non-terrestrial networks,” *IEEE Journal of Microwaves*, vol. 1, no. 3, pp. 704–722, 2021.

[14] Y. Aslan, A. Roederer, N. Fonseca, P. Angeletti, and A. Yarovoy, “Orthogonal versus zero-forced beamforming in multibeam antenna systems: review and challenges for future wireless networks,” *IEEE Journal of Microwaves*, vol. 1, no. 4, pp. 879–901, 2021.

[15] H. Mohammadnezhad, R. Abedi, and P. Heydari, “A millimeter-wave partially overlapped beamforming-MIMO receiver: Theory, design, and implementation,” *IEEE Transactions on Microwave Theory and Techniques*, vol. 67, no. 5, pp. 1924–1936, 2019.

[16] S. Mondal and J. Paramesh, “A reconfigurable 28-/37-GHz MMSE-adaptive hybrid-beamforming receiver for carrier aggregation and multi-standard MIMO communication,” *IEEE Journal of Solid-State Circuits*, vol. 54, no. 5, pp. 1391–1406, 2019.

[17] S. Golabighezelahmad, E. Klumperink, and B. Nauta, “A 1-4 GHz 4×4 MIMO receiver with 4 reconfigurable orthogonal beams for analog interference rejection,” in *IEEE Radio Frequency Integrated Circuits Symposium (RFIC)*, 2019, pp. 339–342.

[18] C. A. Guo and Y. J. Guo, “A general approach for synthesizing multibeam antenna arrays employing generalized joined coupler matrix,” *IEEE Transactions on Antennas and Propagation*, vol. 70, no. 9, pp. 7556–7564, 2022.

[19] C. A. Guo, Y. J. Guo, H. Zhu, W. Ni, and J. Yuan, “Optimization of multibeam antennas employing generalized joined coupler matrix,” *IEEE Transactions on Antennas and Propagation*, vol. 71, no. 1, pp. 215–224, 2023.

[20] R. Vergez, Y. Aslan, A. Roederer, and A. Yarovoy, “A novel butler-enhanced 2 beam by 4 element analog beamforming network,” in *IEEE Conference on Antenna Measurements and Applications (CAMA)*, 2023.

[21] A. Roederer, Y. Aslan, N. J. G. Fonseca, P. Angeletti, and A. Yarovoy, “Multiple beam forming networks for antennas with interference mitigation functionality,” NL patent application nr. 2035700, filed on Aug. 29, 2023.

[22] Y. Aslan, A. Roederer, and A. Yarovoy, “System impacts of user scheduling with minimal angular separation constraints in radio resource management for 5G and beyond,” in *IEEE Asia-Pacific Microwave Conference (APMC)*, 2020, pp. 724–726.

[23] *TLY-5 avionics & aerospacegrade very low DK base material*, AGC Inc., 2023.